LANGMUIR

Article

pubs.acs.org/Langmuir

Mechanism of Reversible Peptide−Bilayer Attachment: Combined Simulation and Experimental Single-Molecule Study

Nadine Schwierz,[*,†] Stefanie Krysiak,[‡] Thorsten Hugel,[‡,§] and Martin Zacharias[∥]

[†]Chemistry Department, University of California, Berkeley, California 94720, United States

[‡]NIM and IMETUM and [∥]Physik-Department, Technische Universität München, 85748 Garching, Germany

[§]Institute of Physical Chemistry, University of Freiburg, 79104 Freiburg, Germany

Supporting Information

ABSTRACT: The binding of peptides and proteins to lipid membrane surfaces is of fundamental importance for many membrane-mediated cellular processes. Using closely matched molecular dynamics simulations and atomic force microscopy experiments, we study the force-induced desorption of single peptide chains from phospholipid bilayers to gain microscopic insight into the mechanism of reversible attachment. This approach allows quantification of desorption forces and decomposition of peptide−membrane interactions into energetic and entropic contributions. In both simulations and experiments, the desorption forces of peptides with charged and polar side chains are much smaller than those for hydrophobic peptides. The adsorption of charged/polar peptides to the membrane surface is disfavored by the energetic components, requires breaking of hydrogen bonds involving the peptides, and is favored only slightly by entropy. By contrast, the stronger adsorption of hydrophobic peptides is favored both by energy and by entropy and the desorption forces increase with increasing side-chain hydrophobicity. Interestingly, the calculated net adsorption free energies per residue correlate with experimental results of single residues, indicating that side-chain free energy contributions are largely additive. This observation can help in the design of peptides with tailored adsorption properties and in the estimation of membrane binding properties of peripheral membrane proteins.

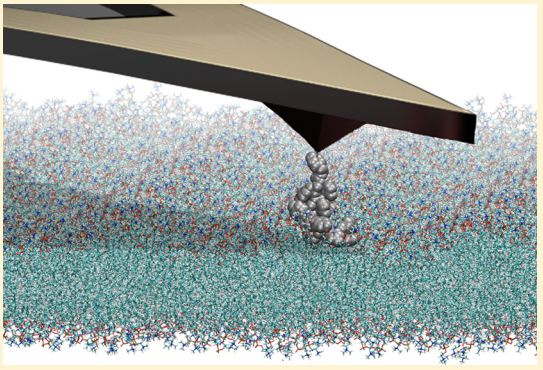

INTRODUCTION

Protein−membrane interactions are important since they govern a large variety of vital cellular processes. Examples include cell signaling and transport,[1,2] blood coagulation,[3] biological activation,[4] pore formation,[5] and neurodegenerative diseases.[6] Binding of surface-active peptides and proteins to the membrane can destroy invasive microorganisms,[7,8] inhibit or promote membrane fusion,[9,10] and cleave the lipid molecules in inflammation response.[11]

A large number of cytosolic proteins, known as peripheral membrane proteins, can bind reversibly to membranes using different strategies.[2] At zwitterionic membranes the forces driving this reversible adsorption are weak noncovalent bonds, notably van der Waals forces, hydrogen bonds, hydrophobic interactions, and solvent-mediated interactions.[12] Protein adsorption depends, among other conditions, on the protein conformation and sequence,[13,14] membrane properties,[15−17] and solvent conditions such as pH,[18] salt concentration,[19] and temperature.[20] These components oppose or favor protein adsorption, but typically lead to near cancellation of the individual contributions, and typical association energies per residue do not exceed a few k_BT.[16,21,22] Moreover, proteins can undergo structural changes upon membrane binding. The protein binding process can involve rearrangements in the membrane and the surrounding water molecules which can complicate the analysis of protein membrane interactions. In order to systematically investigate protein and peptide adsorption at membranes, it is therefore useful to focus on simple model systems. In the first step of a bottom-up approach to control and manipulate protein−membrane interactions, short polypeptides are a particularly suitable model system for designing peptides with tailored functionalities that may be exploited for therapeutic applications.[23]

Important insights into the influence of surface properties on the peptide adsorption behavior come from adsorption studies at the solid/water interface. There, adsorption increases with increasing surface hydrophobicity and with increasing side-chain hydrophobicity of the peptide.[16,17,24,25] However, synthetic surfaces are well-defined rigid structures with controlled overall hydrophilic or hydrophobic surface properties. The situation is more complex in the case of peptides interacting with membranes since membranes are dynamic structures and contain spatially varying hydrophilic and hydrophobic elements. It is far from clear if the same

Received: September 14, 2015
Revised: December 22, 2015
Published: December 30, 2015

DOI: 10.1021/acs.langmuir.5b03435
Langmuir 2016, 32, 810−821

observations and conclusions derived from peptide interactions with solid surfaces hold for peptide interactions with membrane surfaces.

The interaction of peptides with membranes can also be compared with the solubility of amino acid side chains in organic solvents or the partitioning of protein residues between polar and apolar solvents.[26,27] Since a membrane surface contains polar and apolar chemical groups, the interaction with peptides can be considered as a partitioning of residues in hydrophilic and hydrophobic core regions of the membrane.[28−30] The propensity of different amino acids for the hydrophobic core of a membrane and the interfacial region has been determined experimentally by White and co-workers[27,28,31] with a focus on the localization and folding of surface active peptides. Their experimental work has subsequently been complemented by simulations of the identical system[32] and of single amino acids.[33]

A variety of calorimetric and spectroscopic techniques such as nuclear magnetic resonance (NMR), electron parametric resonance (EPR), X-ray diffraction, and electron microscopy (EM) have been used to characterize structural and thermodynamic properties of peptide−membrane interactions.[34−39] These techniques can help to elucidate average structural properties and thermodynamic quantities of peptide−membrane complexes. In addition, atomic force microscopy (AFM) offers the possibility to investigate the reversible attachment of peptides to membranes and to measure desorption forces on the level of single molecules.[16,22,40] The combination of AFM experiments and closely matched molecular dynamics (MD) simulations allows the interpretation of spatially resolved desorption forces and the investigation of the microscopic origin of energetic and entropic contributions to peptide−membrane interactions. Previously, the combined AFM and MD approach has been applied successfully to investigate individual contributions to hydrophobic interactions,[22] temperature dependence,[20] and free energy of adsorption of materials-binding peptides[40] as well as adsorption and adsorption resistance at self-assembled monolayers.[16]

In the current work, we apply this combined approach to model systems consisting of short homopolypeptides and a phospholipid bilayer to gain insight into the mechanism of reversible peptide−bilayer attachment. The zwitterionic phospholipid bilayer consists of dioleoyl-*sn*-phosphatidylcholine (DOPC) headgroups. The focus on homopolypeptides allows us to elucidate amino acid specific effects which are more difficult to extract from peptides with mixed sequences. Our results show a close match between the MD simulations and AFM experiments: In dynamic pulling experiments and simulations, we analyze the rupture forces with varying loading rate. In an intermediate regime of pulling velocities, experimental and simulated rupture forces show the same scaling with the logarithm of the pulling velocity. In this regime, experiments and simulations are simultaneously described by the Bell−Evans model with the same parameters. Further simulations in the limit of vanishing pulling velocities allow a quantitative comparison to the average desorption forces derived from experiments. In both simulations and experiments, hydrophobic peptides preferentially adsorb at the lipid/water interface and the desorption forces increase with increasing side-chain hydrophobicity. The MD simulations are used to determine energetic and entropic components to the peptide−membrane interactions: for the charged and polar peptides, membrane adsorption is disfavored by the energetic components and favored slightly by entropy. In particular, the energetically unfavorable adsorption is reflected in the loss of hydrogen bonds in the membrane bound state. For the hydrophobic peptides, both energetic and entropic contributions favor adsorption and the average number of hydrogen bonds in the membrane adsorbed state exceeds those formed in the bulk solvent. Surprisingly, the adsorption mechanism for hydrophobic peptides at the bilayer surface is similar to the adsorption mechanism at solid hydrophobic surfaces,[16] explaining common trends observed in these vastly different systems.

METHODS

Simulations. Molecular dynamics simulations are performed in the isothermal isobaric (*NPT*) ensemble with fixed particle number N, with a constant ambient pressure P = 1 bar, and at constant temperature T = 300 K using the Gromacs simulation package.[41] The particle-mesh Ewald method is used for the periodic treatment of Coulomb interactions, and bonds to hydrogen atoms are constrained by using LINCS.[42]

Bilayer. The lipid bilayer consists of 128 1,2-dioleoyl-*sn*-phosphatidylcholine (DOPC) molecules. The initial coordinates are obtained using the CHARMM-GUI (http://www.charmm-gui.org) and the force field parameters of the bilayer are taken from CHARMM version C36 due to good agreement with experimental results.[43] This force field has been designed for simulations of lipids and protein systems[44,45] and has been applied and tested in extensive MD simulations[46] and free energy simulations of lipid/peptide systems.[47] The bilayer and 5763 TIP3P water molecules are pre-equilibrated in an *NPT* simulation with isotropic pressure coupling. Initially the pressure is coupled separately to the x/y- and z-directions using a compressibility of 4.5 × 10^{-5} bar^{-1}. For the subsequent NAP_zT simulations with anisotropic pressure coupling, we select a configuration with surface area 67.4 $Å^2$ per lipid and a bilayer thickness of 3.815 nm to match the experimental value for the area per lipid.[48] Thereby, the average bilayer thickness is defined as the lateral distance between phosphate groups in the upper and lower bilayer leaflet. In the following the zero point corresponding to the lipid/water interface is defined by the average position of the phosphor groups in the upper leaflet. Figure 2A shows a simulation snapshot of the phospholipid bilayer, and Figure 2B shows the density of the individual bilayer groups perpendicular to the interface.

Homopolypeptides. We use the homopolypeptides consisting of either glutamic acid (glu), glutamine (gln), lysine (lys), alanine (ala), valine (val), tryptophan (trp), tyrosine (tyr), leucine (leu), or phenylalanine (phe). All uncharged homopeptides consist of 12 amino acids, and the charged peptides glu and lys consisted of 11 amino acids. We choose alternating uncharged and charged variants of the residues since according to the pK values of these peptides the degree of dissociation is reduced to 0.5 at neutral pH (pK_a = 4.25 for glutamic acid and pK_b = 10.53 for lysine). Note that charge regulation close to a low dielectric constant substrate leads to a further decrease of the fraction of charged monomers.[49,50] To obtain an overall neutral system, Na^+ or Cl^- counterions are added to the water phase. The amino acid termini are capped to mimic an infinite peptide chain and to prevent interactions of charged amino or carboxyl moieties with the surface. The N-terminus is terminated with an uncharged amino group, while the C-terminus is terminated with a carboxyl group. The force field parameters for the peptides are taken from CHARMM version C27. Initially, the peptide is placed in the simulation box above the equilibrated bilayer before it is filled with TIP3P water.

Forced Adsorption. In order to probe the barrier for bringing a peptide chain into the interfacial region, we perform constant force simulations. In these simulations, an additional constant external force $F_{Ext} = m_i a$, where m_i is the mass of each atom and a is the constant acceleration acting toward the surface, is applied to the peptide in the $-z$-direction during a 20 ns NAP_zT simulation. For the acceleration we chose values between 0.00083 and 1 nm/ps^2. For each simulation, the average separation d_z of the peptide from the surface is calculated as

DOI: 10.1021/acs.langmuir.5b03435
Langmuir 2016, 32, 810−821

the mean value of the separation of all atoms, using the last 5 ns. The work of adhesion necessary to bring the peptide from bulk to an average separation d_z from the interface is calculated by integrating the force along d_z:

$$A(d_z) = \int_{d_z}^{\infty} F_{\mathrm{Ext}}(d_z')\, \mathrm{d}d_z' \tag{1}$$

Forced Desorption. To equilibrate the system, we first perform an energy minimization of the system. The subsequent simulation routine consists of four steps. First, we perform constant force simulations, in which the peptide is accelerated toward the bilayer by a constant acceleration of 1 nm/ps^2. For each peptide, we perform one force free control simulation, in which the peptide is positioned close to the interface. From the acceleration trajectory, five to seven configurations with different penetration depths are selected. Subsequently, the acceleration is turned off and the system is allowed to relax in a 20 ns NAP_zT simulation employing Nosé–Hoover temperature coupling with time constant $\tau_T = 0.5\mathrm{s}^{-1}$ and semi-isotropic Parrinello–Rahman pressure coupling with time constant $\tau_p = 1\ \mathrm{s}^{-1}$. Prior to this relaxation simulation we employ a 200 ps NVT and NAP_zT simulation as pre-equilibration using the Berendsen scheme. During the relaxation most of the peptide remains at the lipid/water interface. Third, dynamic pulling simulations are performed for at least five different, initially adsorbed, starting configurations. In the pulling simulations mimicking AFM experiments the peptide is pulled vertically away from the interface with constant pulling velocity. To manipulate the peptide, a harmonic restraint potential with spring constant k = 166 pN/nm is applied on the z-coordinate acting only on the last residue of the peptide (C-terminus) and leaving the lateral coordinate unperturbed. The center of the restraint potential is moved with constant velocity v in the z-direction perpendicular to the interface and the force is calculated. The zero point of the z-coordinate is defined by the mean position of the phosphate groups. The pulling is done until the peptide is completely desorbed from the interface. Fourth, static simulations are performed in which the restraining potential is kept at a fixed position for 29 ns. The starting configurations are obtained from two randomly chosen dynamic simulations at v = 0.1 m/s pulling rate. The static simulations are performed for all elongations from the adsorbed state to the desorbed state with a step size of 0.2 nm. Note that peptide penetration into the membrane in general involves large-scale deformations and reorientation of the membrane and therefore requires long equilibration.[51] Low forces in the forced adsorption setup that do not disrupt the membrane, and a subsequent equilibration allowing rearrangement of the membrane is therefore crucial for a convergence of the results.

The free energy is calculated by integrating the force along the pulling path. The internal energy and the different contributions are extracted as the time average of the static simulations, discarding the first 5 ns for equilibration. In order to obtain the energy difference between the surface adsorbed state and the desorbed bulk state, the static simulations are split accordingly. The average energy of each state is then calculated as a weighted average over all surface adsorbed and all bulk configurations. Insight into the various energetic contributions stemming from interactions between peptide (P), water (W), and surface (S) can be gained from the simulations. In a simulation rerun, the system is divided into the different components and the energies of the individual groups are calculated. The individual energetic contributions sum up to the total energy U according to $U = U_{\mathrm{PP}} + U_{\mathrm{WW}} + U_{\mathrm{PS}} + U_{\mathrm{SW}} + U_{\mathrm{PW}} + U_{\mathrm{SS}}$. The total enthalpy can be calculated from $H = U + pV$. However, a decomposition of the pV term, the total desorption free energy, or the entropy into individual contributions is not feasible. Further information on the energy decomposition is given in the Supporting Information.

Rupture Forces at Low and High Loading Rates. In the dynamic pulling experiments and simulations, the spring is moved away from the bilayer at constant velocity, building up mechanical stress in the system. Eventually, the applied force leads to a molecular transition such as the desorption of the peptide from the surface. Both simulations and experiments allow measurement of the mean force at rupture or the most probable force at rupture. Typically, the pulling velocities of experiments and simulations differ by several orders of magnitude, leading to a different scaling of the rupture forces with pulling velocity. For low pulling velocities that are in the range of our experiments, the following empirical relation between the most probable rupture force F_{max}, the intrinsic rate constant in the absence of pulling k_0, the harmonic force constant k_S, and the distance from the free energy minimum to the barrier $x^{\ddagger}$ exists:[52,53]

$$\beta F_{\mathrm{max}} \approx \frac{1}{x^{\ddagger}} \ln(k_S v x^{\ddagger} k_0^{-1}) \tag{2}$$

where $\beta = 1/k_BT$. A similar relation can be obtained for the mean rupture force $\bar{F}$. Note that eq 2 is valid in the classical dynamic force spectroscopy regime where the force increases linearly with the logarithm of the loading rate. In this regime, the force spectra taken with different cantilever stiffnesses collapse on a single line[54] and the peaks in the force spectra correspond to the rupture of a single or a few molecular bonds and the rupture force is therefore largely independent of the length of the peptide chain. In the limit where eq 2 is valid, the difference between the maximum of the force distribution and the mean rupture force is given by

$$F_{\mathrm{max}} - \bar{F} = k_B T \gamma / x^{\ddagger} \tag{3}$$

where γ is the Euler–Mascheroni constant.[55] In the regime of low loading rates the rupture force grows linearly with the logarithm of the force-loading rate $F_{\mathrm{max}} \sim \ln(k_S v)$.

For sufficiently fast pulling velocities that are in the range of our simulations, the mean rupture force $\bar{F}$ is proportional to the square root of the velocities:[55]

$$\beta \bar{F}(v \to \infty) \sim v^{1/2} \tag{4}$$

Note that the analytical expressions above are obtained assuming that the system diffuses on a harmonic free energy surface with a single sharp barrier and is pulled by a harmonic spring moving with constant velocity. To test the predicted scaling behavior, we perform experiments and simulations with different pulling velocities. The details on the experiments are given further below. The simulations are performed with four different velocities (v = 0.01, 0.1, 1, 10 m/s) using the dynamic pulling protocol described previously. For each simulation the rupture force is determined from the maximum force over the full desorption path. For each velocity, the rupture force and the standard deviation are determined. For a consistent definition of experimental and simulated loading rates, the instantaneous (local) loading rate at rupture is calculated from a linear fit to the force–time curve in the vicinity of the maximal force (see Figure S5D in the Supporting Information for an illustration). In the dynamic pulling simulations, the harmonic spring constant k_s = 166 pN/nm used.

Experiments. *Bilayer.* DOPC and 18:1 Liss Rhod PE were purchased from Avanti Polar Lipids. DOPC and 18:1 Liss Rhod PE are mixed in chloroform at a molar ratio 2000:1. Chloroform is evaporated from the lipid mixture samples in a gentle nitrogen gas stream, and afterward the samples are placed in a vacuum for 1 h. The lipids are solvated at 2.5 mg/mL in ultrapure water, and the mixture is extruded using the Avanti Mini Extruder with polycarbonate membranes of pore size 100 nm. The vesicle solution is diluted 1:5 (0.5 mg/mL) and $CaCl_2$ is added to a concentration of 3 mM. Mica is glued to a glass slide and inserted into a fluid cell together with a hydrophobic control substrate (PTFE). Mica is then freshly cleaved and a droplet of 100 μL vesicle solution is incubated on the mica for 10 min before the sample is rinsed with ultrapure water. The sample is then placed in an oven at 50 °C to get rid of potentially remaining adherent vesicles. The formation of the bilayer is confirmed by looking at the fluorescence in a microscope. The sample is slowly rinsed with the measurement buffer of 10 mM Hepes and 50 mM NaCl at pH 7 and then placed in the AFM.

Tip Functionalization. For the measurements, polyamino acids are covalently coupled to silicon nitride MLCT cantilevers (tip radius 20 nm, Bruker SPM probes, Camarillo, USA). MLCT cantilevers are activated in an oxygen plasma (20 W, 0.28 mbar) for 15 min. They are then rinsed with dry acetone and incubated in Vectabond solution for

DOI: 10.1021/acs.langmuir.5b03435
Langmuir 2016, 32, 810–821

silanization (50 μL of Vectabond in 2.5 mL of dry acetone) for 10 min and rinsed again twice in dry acetone and once in dry chloroform before being placed in a poly(ethylene glycol) (PEG) mix consisting of 1:1500 PEG-α–ω-DiNHS (6 kDa, Rapp Polymere GmbH, Tübingen, Germany) and CH_3O-PEG-NHS (5 kDa, Rapp Polymere GmbH, Tübingen, Germany) prepared in dry chloroform. After 45 min of incubation they are rinsed in dry chloroform, ethanol, and 50 mM sodium borate buffer pH 8.1 (for poly-D-tyrosine and poly-L-glutamic acid functionalization) or dry DMSO (for poly-L-tryptophan functionalization). Then, they are placed in 1 mg/mL polyamino acid solved in 50 mM sodium borate buffer pH 8.1 or dry DMSO respectively and incubated for 1 h and rinsed in sodium borate buffer or DMSO and ultrapure water. The polymers poly-D-tyrosine (40–100 kDa), poly-L-tryptophan (15–50 kDa), and poly-L-glutamic acid (50–100 kDa) were purchased from Sigma-Aldrich. PEG tips are functionalized following the activation and silanization steps of the protocol above but using only CH_3O-PEG-NHS instead of a PEG mix.

AFM Measurements. The AFM force spectroscopy measurements are carried out with an MFP3D equipped with a fluid cell at room temperature. As measurement buffer 10 mM Hepes and 50 mM NaCl at pH 7 is chosen. At the beginning of the measurement, the inverse optical lever sensitivity (InvOLS) of the functionalized cantilever is determined from the indentation slope on PTFE and the spring constant calibrated with the thermal noise method. Successful functionalization of the tip is confirmed by constant force plateaus on PTFE. Then, a tapping mode image of the DOPC bilayer is made with the same cantilever. A spot covered with a DOPC membrane is chosen in the image for force spectroscopy measurements. The tip velocity is 1 μm/s, the indentation force is 300–500 pN, and the dwell time is 4 s. A number of force–distance traces are recorded followed by a tapping mode image to confirm that the measurement spot is still on the bilayer. Then, a new spot is chosen and some more force–distance traces are recorded. In this fashion a total of at least 644 extension–retraction cycles are recorded for each experiment. At the end of the experiment the InvOLS is determined again on PTFE and a second thermal noise spectrum is measured. As a control, the experiment as described above is also carried out with a PEG tip and no events with a distance larger than 15 nm are recorded. For details see Figure S5A,B in the Supporting Information. For polytyrosine and polytryptophan, additional force curves are recorded for retraction speeds 0.1 and 10 μm/s.

Data Analysis. The InvOLS and spring constant calibrated at the beginning and at the end of the experiment are averaged and used to compute the force–distance traces for the whole experiment. The data handling and analysis is done in Igor Pro. Force curves are automatically analyzed for interaction events. To exclude nonspecific effects from the tip–surface interaction, events closer than 15 nm to the surface are excluded. The averaged force is extracted from each force–distance curve. The averaging is taken starting at the distance 15 nm from the surface until the rupture distance at which the force dropped to zero (Figure S5C). The averaged forces of all force–distance traces of a single homopolypeptide are plotted in a histogram. Beforehand, we ensured that the detachment lengths of the three different homopolypeptides are similar (for details see the Supporting Information). The averaged force histograms are fitted with a Gaussian function allowing extraction of the peak value as well as the standard variation. For polytyrosine and polytryptophan dynamic force spectroscopy is performed with measurements at three different retraction velocities. For those measurements, the maximal peak force value is determined (Figure S5C). The value is averaged over 10 data points to get a value independent of the noise level. The instantaneous loading rate is determined by plotting the force trace against time and fitting 50 points before the maximal force peak with a line. The slope of the fit is the loading rate. This is illustrated in Figure S5D in the Supporting Information.

Loading Rate and Rupture Force. To test the velocity dependence of the polypeptide desorption from the bilayer, measurements with three different pulling velocities of 0.1, 1, and 10 μm/s are performed with polytyrosine and polytryptophan. Due to the low number of desorption events, this measurement is not possible in a reasonable time frame with polyglutamic acid. The dwell time on the surface is chosen to be 4 s, and the trigger force is 500 pN. The instantaneous loading rate at rupture is determined by a linear fit to the force–time curve in the vicinity of the maximal force. This is a valid approximation since the highest probability for the bond to break is at higher forces, so the last part of the curve is most important. The maximal force is determined from the highest force peak in each force–extension curve. This can be the last interaction of the trace (detach force), or it can be followed by a stick or slip of lower force. The analysis of the force curves is illustrated in Figure S5 in the Supporting Information. The loading rates for the four different pulling velocities are broadly distributed and even overlap. The data points are sorted into four groups depending on loading rate ($<10^{-10}$, 10^{-10}–10^{-9}, 10^{-9}–10^{-8}, $>10^{-8}$ N/s). Histograms of the maximal forces are plotted for each loading rate range. From each force histogram the most probable force is extracted. The average loading rate for the data points in each group is calculated together with the standard variation. A constant loading rate (force ramp) is assumed, and by setting the derivative of the probability to be bound at force F to zero, an expression for the most probable rupture force as a function of loading rate r_F is calculated using the Bell–Evans model:[53] $F_{max} = \frac{1}{\beta x^{\ddagger}} \ln\left(\frac{x^{\ddagger} r_F}{k_0}\right)$. Here k_0 denotes the transition rate at zero force and $x^{\ddagger}$ is the distance between bound and transition states. Note that this expression is equivalent to eq 2 with the instantaneous loading rate r_F determined for each curve separately. If the attempt frequency A is known, the activation free energy of the reaction barrier $\Delta G^{\ddagger}$ can be calculated from the transition rate following the Bell model:[56] $\Delta G^{\ddagger} = k_B T \ln\left(\frac{A}{k_0}\right)$.

RESULTS AND DISCUSSION

Forced Peptide Adsorption and Interfacial Configuration. In order to bring the peptide to the surface without disrupting the bilayer, we perform constant force simulations in which we uniformly push the peptide toward the surface using different magnitudes of an external force acting on each atom. This simulation setup is equivalent to the experimental setup since on the length scale of the peptide the cantilever is flat. For different values of the external force F_{Ext} the resulting average separation of the peptide from the surface d_z is measured (Figure 1A). The forces required to push the peptide onto the bilayer are 100–400 pN and increase with increasing size of the side chain. In the experiment, the forces that are used to push the peptide onto the lipid bilayer are in a comparable range, namely 300–500 pN. These forces are large enough to observe adhesion events but low enough not to puncture the membrane.

Figure 1B indicates the work of adhesion necessary to bring the peptide chains from bulk to a desired average separation d_z from the interface. The dashed line in the plot corresponds to a fit for tyrosine to the change of an elastic medium with the elastic modulus of DOPC at room temperature.[57] It is assumed that the area of the stretched bilayer is proportional to the square of peptide penetration, $A \sim k_A(d_z - d_0)^2$ with k_A = 153.9 kJ/mol nm^2. Hence, applying a low, constant force to the peptide results in an elastic deformation of the bilayer and is therefore suitable to initiate peptide adsorption in the simulations and in the experiments.

To investigate the interfacial partitioning in more detail, we determine the probability distribution of the different peptides perpendicular to the interface after a 20 ns relaxation simulation using at least five different starting configurations. The probability distribution of all peptides is shown in Figure 2C, where the points indicate the starting configuration. During this relaxation the elastically deformed bilayer relaxes back into its

DOI: 10.1021/acs.langmuir.5b03435
Langmuir 2016, 32, 810–821

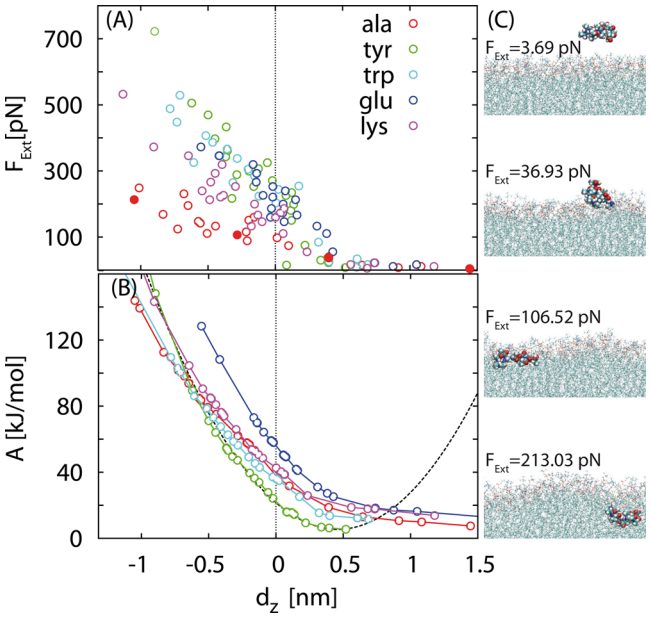

Figure 1. Simulation results for the forced adsorption: external constant force F_{Ext} is used to bring the peptides from bulk water to the lipid/water interface. (A) External force F_{Ext} and (B) work of adhesion A in dependence of the average lateral distance from the bilayer for selected peptides. The vertical dotted lines indicate the position of the interface. Solid red points indicate the values of the external force F_{Ext} for which the snapshots in (C) are taken. The dashed line in (B) is the free energy change of an elastic medium with elastic modulus appropriate for a DOPC bilayer. The offset is fitted to the free energy curve of tyrosine. (C) Simulation snapshots for alanine using different values for the external force F_{Ext}. Water molecules are not shown for clarity.

initial configuration and most of the peptides remain adsorbed. However, the polar peptides (shades of blue, Figure 2C) have a higher propensity to spontaneously desorb into bulk compared to the more hydrophobic peptides (shades of red, Figure 2C). This is in agreement with our experimental findings where the probability to measure adhesion events is a factor of 10 lower for the charged glutamic acid than for the hydrophobic tryptophan and tyrosine (see Figure S6 in the Supporting Information). Figure 2D–F provides further insight into the interfacial configuration and preferential interaction sites for tyrosine, tryptophan, and glutamic acid. These individual fingerprints show the lateral average center of mass distance of each amino acid from the interface for the different starting configurations after relaxation. The hydrophobic tyrosine preferentially interacts with hydrophobic tails, tryptophan interacts both with hydrophobic tails and hydrophilic headgroups, and glutamic acid prefers interaction with hydrophilic headgroups or desorbs spontaneously into the polar solvent.

Rupture Force in Dependence of the Loading Rate in Experiments and Simulations. We now turn to the dynamics of peptide desorption from the lipid bilayer. We start the discussion with the results from nonequilibrium pulling by investigating the rupture forces in dependence of the loading rate obtained in the experiments (low loading rates) and in the simulations (high loading rates). The rupture force in dependence of the loading rate obtained in the AFM experiments is shown in Figure 3A,B for tryptophan and tyrosine. Different colors indicate the three different pulling velocities (0.1–10 μm/s). The individual data points from each measurement are sorted into four blocks according to the loading rate, and the most probable rupture force F_{max} (maximum of the force distribution) of each block is calculated (large red points in Figure 3). The data is fitted according to eq 2 in the low loading rate regime of the experiments to further provide insight into the interaction range $x^{\ddagger}$ (equivalent to the position of the barrier). For tryptophan, $x^{\ddagger}$ = 0.65 nm, and for tyrosine $x^{\ddagger}$ = 0.62 nm. Both values are large compared to typical values for covalent bonds (0.1–0.2 nm) and more consistent with long-ranged, noncovalent interactions. The

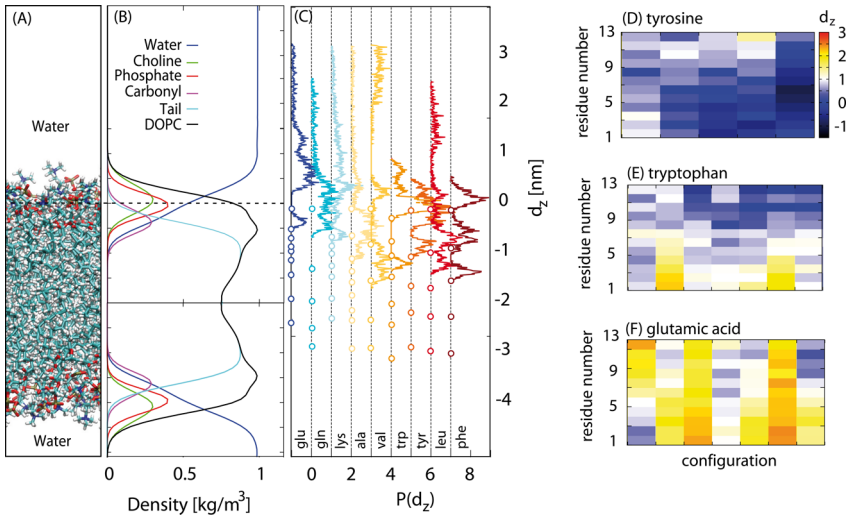

Figure 2. (A) Simulation snapshot of the lipid DOPC bilayer. (B) Density of individual bilayer groups perpendicular to the interface. (C) Probability distribution of all peptides perpendicular to the interface measured by the center of mass distance between the peptide and the lipid/water interface d_z. The distribution is obtained after a 20 ns relaxation by using different starting configurations obtained by forced adsorption. The initial center of mass distance between peptide and bilayer is indicated by open circles. Individual fingerprints for (D) polytyrosine, (E) polytryptophan, and (F) polyglutamic acid. Each block shows the average distance of each amino acid from the interface. The rows correspond to the different starting configurations indicated by the open circles in (C). Blue corresponds to side chains deep in the bilayer interacting with the hydrophobic tails, white corresponds to side chains in the region of the hydrophilic headgroups, and yellow corresponds to side chains that are desorbed in water.

DOI: 10.1021/acs.langmuir.5b03435
Langmuir 2016, 32, 810–821

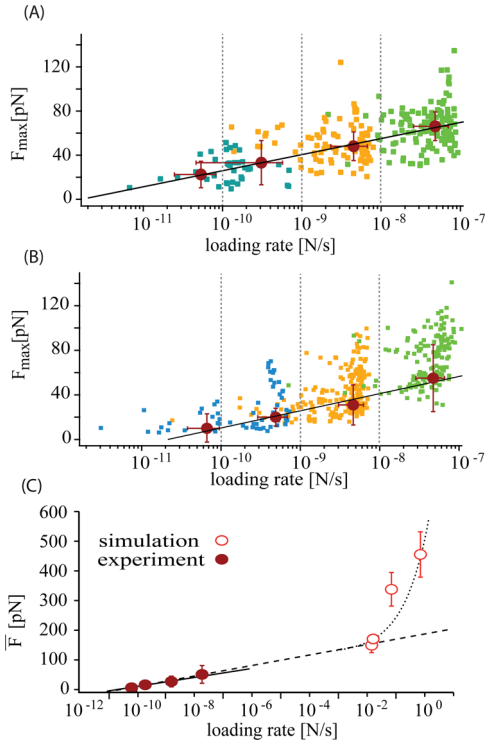

Figure 3. Maximal force value and corresponding instantaneous loading rate of each curve of the experimental polytryptophan (A) and polytyrosine (B) measurements on DOPC plotted in a linear against logarithmic graph. The data collected with pulling velocity 0.1 μm/s is plotted in blue, the 1 μm/s data is plotted in yellow, and the 10 μm/s data is plotted in green. The data points are sorted into four bins depending on loading rate ($<10^{-10}$, 10^{-10}–10^{-9}, 10^{-9}–10^{-8}, $>10^{-8}$ N/s) as denoted by dotted lines. The most probable rupture force F_{max} is determined for each bin and plotted against the average loading rate of the range (red dots). Those data points are fitted with the Bell–Evans model (black line) yielding $x^{\ddagger} = 0.65 \pm 0.02$ nm and $k_0 = 0.27 \pm 0.007$ Hz (tryptophan) and $x^{\ddagger} = 0.62 \pm 0.09$ nm and $k_0 = 3.2 \pm 1.9$ Hz (tyrosine). (C) The mean forces at rupture $\overline{F}$ dependent on the instantaneous loading rates of experimental polytyrosine measurements are plotted together with the corresponding results from the simulations. The solid black line corresponds to the fit to experimental data (same as in (B) with offset according to eq 3). The dashed line shows a simultaneous fit of the experimental data and the simulation results for the two lowest pulling velocities ($v \leq 0.1$ m/s). In this intermediate regime, both simulations and experiments show the same scaling with the logarithm of the loading rate and can be described simultaneously. At high loading rates in the regime of the two fastest pulling simulations ($v \geq 1$ m/s), the average rupture force increases with the square root of the pulling velocity (shown as dotted line).

intrinsic rate constants are $k_0 = 0.27 \pm 0.07$ Hz for tryptophan and $k_0 = 3.2 \pm 1.9$ Hz for tyrosine.

From these values it is possible to estimate the activation free energy or energy barrier of the bond if the Arrhenius prefactor A is known. The effective monomeric desorption rate of polytryptophan on a hydrophobic surface is reported to be on the order of 10^5 Hz for polytyrosine.[58] A monomer here means a unit of the size of the Kuhn length (0.7 nm), that is, about 1.5–2 residues on a polypeptide chain. Using this value as the Arrhenius prefactor yields activation free energies of $13k_BT$ for polytryptophan and $10k_BT$ for polytyrosine. It should be noted that those values have a high uncertainty due to the fit procedure and the choice of the Arrhenius prefactor.

Nonequilibrium Rupture Forces: Slow and Fast Pulling Regimes in Experiments and Simulations. The pulling velocities of experiments and simulations differ by several orders of magnitude leading to a different scaling of the rupture forces with pulling velocity. The different pulling regimes are evident from Figure 3C, in which the experimental mean forces at rupture $\overline{F}$ from the experiments (calculated from F_{max} according to eq 3) and from the simulations are shown in dependence of the loading rate. For low pulling velocities that are used in our experiments and for the two lowest pulling velocities in the simulations ($v \leq 1$ m/s), the rupture force scales linearly with the logarithm of the loading rate (solid and dashed lines in Figure 3C) as expected from eq 2. By contrast, the rupture forces obtained from the simulations with the two highest pulling velocities ($v \geq 0.1$ m/s) show a different behavior. Here, the mean rupture force is proportional to the square root of the velocities (dotted line in Figure 3C). We conclude that the force induced mechanical transition of membrane adsorbed peptides is in line with the predictions from analytical theory.[55] Moreover, in an intermediate regime experimental and simulated rupture forces show the same scaling with the logarithm of the loading rate. In this intermediate regime, experiments and simulations can be described simultaneously and the force is determined only by the kinetic parameters to rupture noncovalent bonds between peptide and membrane. At large pulling velocities ($v \geq 0.1$ m/s), experiments and simulations are located in different pulling regimes evident from the different scaling of the rupture force with loading rate.

Force–Extension Curves: Dynamic Desorption of Peptides from the Bilayer in Experiments and Simulations. Having obtained insight into the rupture forces and their dependence on the pulling velocity, we now focus on the dynamic desorption of the peptides from the lipid DOPC bilayer using low pulling velocities. In the following, we present the force–extension curves from the experiments and simulations which provide insight into the interaction of peptides with the bilayer.

The force–extension curves for glutamic acid, tyrosine, and tryptophan obtained by the AFM experiments show a variety of curve shapes (Figure 4). This variety of curve shapes is absent in our control measurements on a solid hydrophobic surface. There, an unspecific adhesion peak follows a flat force plateau in most curves (57–80%) as described in the literature.[16] The interaction length of the polypeptides is shorter on DOPC than on the hydrophobic control surface. This could be caused by the on average lower desorption force on DOPC compared to the solid hydrophobic control surface[58] (see Supporting Information for details).

The force–extension curves for the homopeptides on the lipid DOPC bilayer can be classified into four types of curve shapes: plateau, convex stretching, concave stretching, and a combination of stick–slip motives. The frequency of occurrence of the different types for each peptide is given in Figure 4. Note that the numbers for glutamic acid have to be treated with caution since only 11 adsorption events were measured in total.

Flat force plateaus, as depicted in the first line of Figure 4, occurred only rarely. In the plateau regions, the peptide–surface interaction relaxes faster than the cantilever is moved away from the surface. Here, the peptide has a high mobility on the surface (slip motion).

DOI: 10.1021/acs.langmuir.5b03435
Langmuir 2016, 32, 810–821

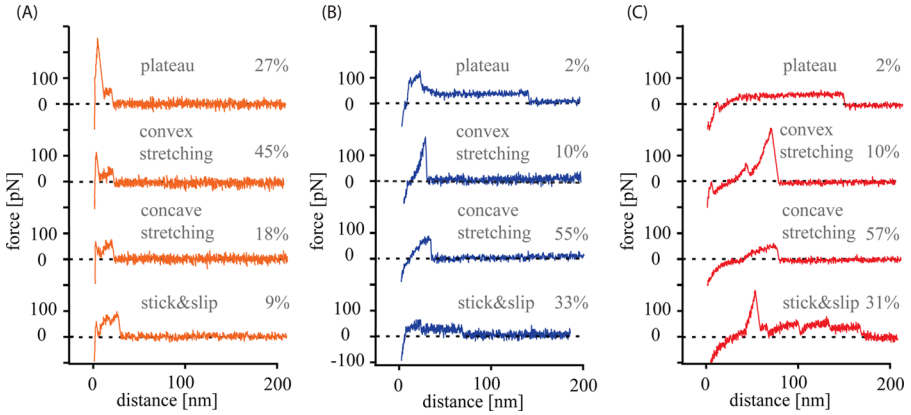

Figure 4. Different curve shapes observed in the experimental desorption curves on DOPC with pulling velocity 1 μm/s. The sample curves of polyglutamic acid are depicted in orange (A), those of polytyrosine are in blue (B), and those of polytryptophan are in red (C). Four motives are observed in the force curves, namely flat plateau forces (first line), convex stretching (second line), concave stretching (third line), and stick and slip motion (fourth line). The percentage of each motive is given. The number of observed events is 11 out of 664 for polyglutamic acid, 227 out of 718 for polytyrosine, and 172 out of 994 for polytryptophan.

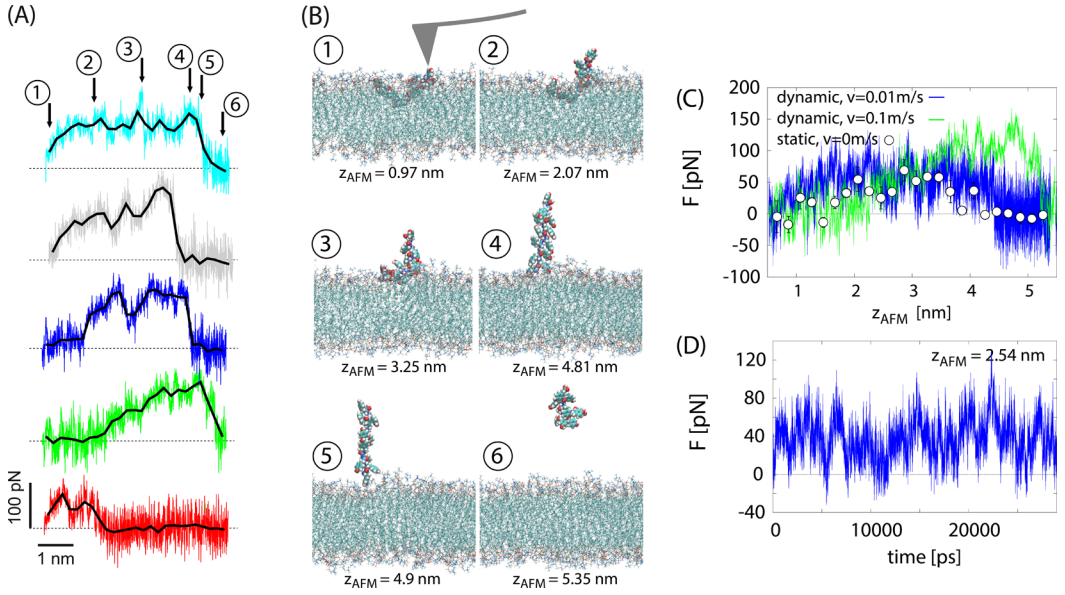

Figure 5. (A) Simulated force–extension curves with pulling velocity v = 0.1 m/s and different starting configurations for polytyrosine. (B) Simulation snapshots of a polytyrosine chain with 12 residues pulled by an AFM. The snapshots are taken for the AFM position z_{AFM} indicated by the arrows in (A). Water molecules are not shown for clarity. (C) Simulated force–extension curve for pulling velocity v = 0.1 m/s and v = 0.01 m/s. Open points denote the results from the static simulations; here the results for the lowest pulling velocity and the static simulations give the same average desorption force. (D) Force as a function of time for the static simulation with z_{AFM} = 2.54 nm separation of the pulled C-terminal and the lipid/water interface.

Convex curve shapes, as shown in the second row of Figure 4, are observed frequently. Here, individual regions are very stable and the relaxation is slow. The peptide is stuck on the surface leading to a stretching of the peptide between the surface and the AFM tip. The stretching can be described by the freely jointed chain or wormlike chain model.[59,60] The stiffness of the coupled system can increase with increasing force, giving rise to the convex shape of the force–extension curve.

Concave curve shapes, as shown in the third row of Figure 4, indicate a deviation from the elastic stretching response and the force–distance curve has concave parts. Examples for such deviations from the elastic stretching response have been reported for biomolecules with conformational changes,[61] the B–S transition of double stranded DNA,[62] or the change from α-helix to planar conformation for stretched PEG.[63]

Combination of the different types is also observed (fourth row of Figure 4). Here, traces show a mixture of peptide slipping, corresponding to the flat plateau regions, and peptide stretching, corresponding to the force spikes. This corresponds to an intermediate situation between slipping and sticking events in which the peptide is either mobile or stuck on the surface.[58,64]

Force–extension curves for tyrosine obtained by simulations using a pulling velocity of 0.1 m/s are shown in Figure 5A. For a better qualitative comparison, the simulated force–extension curves in Figure 5A are averaged to provide the same resolution as the experimental data in Figure 4. We find good agreement between the magnitudes of the forces obtained in the

DOI: 10.1021/acs.langmuir.5b03435
Langmuir 2016, 32, 810–821

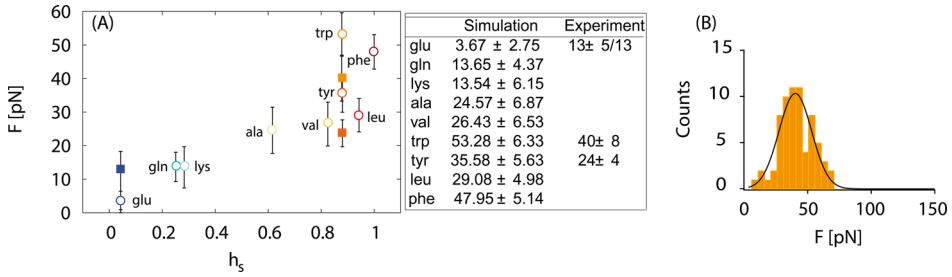

	Simulation	Experiment
glu	3.67 ± 2.75	13± 5/13
gln	13.65 ± 4.37	
lys	13.54 ± 6.15	
ala	24.57 ± 6.87	
val	26.43 ± 6.53	
trp	53.28 ± 6.33	40± 8
tyr	35.58 ± 5.63	24± 4
leu	29.08 ± 4.98	
phe	47.95 ± 5.14	

Figure 6. (A) Simulated average desorption force from the static pulling protocol vs side-chain hydrophobicity scale h_s (open circles). The corresponding experimental average desorption forces for polyglutamic acid, polytryptophan, and polytyrosine are shown as filled squares. All values for the desorption forces are listed in the table on the right. (B) Distribution of the average experimental desorption forces for tryptophan. The hydrophobicity scale is taken from ref 26.

experiments and the simulations. Moreover, the different desorption motives observed in the experiments occur also in the simulated force−extension curves. However, the polypeptides consist of only 11−12 residues in the simulations and the motives occur on a different, much shorter length scale. Still, the simulations can provide further insight into the microscopic origin of the different desorption force motives. For this purpose, simulations snapshots for polytyrosine are shown in Figure 5B. The snapshots are taken for the AFM position z_{AFM} indicated by the arrows in Figure 5A. Initially, the peptide is adsorbed in the interfacial region and interacts preferentially with the hydrophobic tails of the bilayer (see also Figure 2D for the interfacial distribution of tyrosine). Due to the applied force, more and more amino acids are pulled away from the interface and into the water phase until the peptide is stretched between the AFM tip and the bilayer. Interestingly, the membrane shows a small deformation (Figure 5B, snapshot 4) which coincides with a concave part of the force−extension curves. Configurational changes of the membrane could therefore be the reason for the concave shape observed in the experiments.

Mean Desorption Forces in the Stationary Nonequilibrium of Peptide Pulling. A direct comparison of the desorption forces obtained from AFM experiments and MD simulations is challenging due to the different pulling velocities accessible. From the nonequilibrium rupture forces, it is clear that experiments and simulations show the same scaling in an intermediate regime. Still, the pulling velocities differ by several orders of magnitude. However, it is possible to compare the average desorption forces obtained in the simulation to the experimental results by performing simulation in the limit of vanishing pulling velocity (static simulation setup).[16,22] The simulated force−extension curves for different pulling velocities are compared with the static results in Figure 5C. At intermediate pulling velocities of v = 0.1 m/s the desorption process is out of equilibrium. With decreasing pulling velocity the friction effects are diminished and the desorption force decreases. For the lowest pulling velocity, the dynamic results are in good agreement with the static simulations results (open points in Figure 5C which resulted from averaging the force for a fixed surface separation z of the peptides for 29 ns as shown exemplary in Figure 5D). Further information on the dependence of the desorption force on the pulling velocity can be found in the Supporting Information. Both dynamic (v = 0.01 m/s) and static pulling protocols yield an average desorption force of F = 33.95 pN in the static protocol and F = 35.02 pN in the dynamic protocol for polytyrosine. This good agreement demonstrates that dissipative contributions are small and pulling occurs in quasi-equilibrium. Note that in order to reach this quasi equilibrium the pulling velocity is obliged to be 1 order of magnitude slower compared to that used at solid hydrophobic surfaces.[16,22] Thus, the dynamic pulling simulations with v = 0.01 m/s can be compared directly to the experimental data, even though the rates in the AFM experiments are in the micrometers per second range. However, in the following we exclusively use the results obtained from the static simulations for quantitative comparison.

Dependence of the Mean Desorption Forces on Side-Chain Hydrophobicity. The average desorption force from the phospholipid bilayer for all nine homopolypeptides considered in the simulations is compared to the experimental results for glutamic acid, tryptophan, and tyrosine (Figure 6A). The histograms for the experimental desorption forces are shown in Figure 6B for tryptophan and in the Supporting Information. For tryptophan and tyrosine a significant number of forced desorption events could be measured. In the polyglutamic acid measurement, only a small number of traces indicate measurable desorption events (1.5% of recorded traces). Since forces smaller than 10 pN cannot be resolved in our AFM experiments, the experimental value for the desorption force of glutamic acid is overestimated. For all peptides, the desorption forces do not depend on the starting configuration and interfacial penetration (see Table 1 in the Supporting Information). The only exception is tryptophan, for which two different desorption paths occur in the simulations, leading to different desorption forces (F = 41.98 pN and F = 64.59 pN). Consistently, a broader range of desorption forces occurs in the experiments for tryptophan compared to tyrosine (Figure 6B and Figure S6). Note that this broad range of experimental values likely reflects the different desorption forces along the different pathways obtained by the simulations.

In Figure 6A, the average desorption force is plotted as a function of the side-chain hydrophobicity scale h_s derived by Black and Mould.[26] The hydrophobicity scale is based on the partition coefficient, defined as the ratio between the amino acid concentration in octanol and water, and the additivity assumption for all atomic groups. Note that the range of the hydrophobicity scale is rescaled in the range of zero (most polar amino acid) to unity (most hydrophobic residue).

The desorption force in Figure 6A increases with increasing side-chain hydrophobicity. This indicates that the adsorption of the peptides at the lipid/water interface is related to adsorption at the octanol/water interface. The microscopic origin leading to this similar adsorption behavior at fundamentally different interfaces will be discussed in detail further below. An

DOI: 10.1021/acs.langmuir.5b03435
Langmuir 2016, 32, 810−821

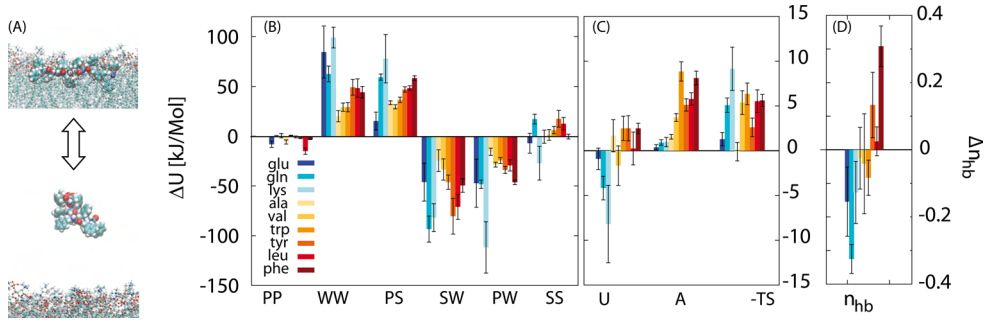

Figure 7. Simulation results at the phospholipid bilayer: energy/entropy difference between the surface adsorbed state and the desorbed bulk state. (A) Illustration of the adsorbed state and the bulk state for polyphenylalanine. (B) Decomposition of the internal energy difference $\Delta U = U(\text{bulk}) - U(\text{surface})$ per monomer of the different homopeptides into interaction contributions involving peptide (P), surface (S), and water (W). The peptides are ordered from left to right according to increasing side-chain hydrophobicity h_s. Charged/polar residues are shown in shades of blue; hydrophobic residues are shown in shades of red. (C) Total internal energy U, free energy of desorption A, and entropic contribution $-TS$. (D) Difference in the number of hydrogen bonds $\Delta n_{hb} = n_{hb}^{ads} - n_{hb}^{des}$ per monomer in the surface adsorbed n_{hb}^{ads} and the desorbed bulk configuration n_{hb}^{des}. All values of the energy decomposition are listed in Table 2 of the Supporting Information.

exceptional and highest value for the desorption force is encountered for tryptophan in agreement with the known preferential interaction of tryptophan with lipid bilayers.[65,66]

Energy and Entropy Decomposition. The forces driving reversible peptide adsorption at zwitterionic lipid bilayers are weak noncovalent interactions, resulting from van der Waals forces, hydrogen bonds, the hydrophobic effect, and other solvent-mediated interactions.[12] These interaction forces are relatively insignificant taken individually and due to the typical near cancellation of the individual contributions among water, surface, and peptide typical association energies are small.[21] Therefore, high precision in each contribution is needed for quantitative correct predictions.

In order to get insight into the mechanism of reversible peptide adsorption, we calculate the energy difference $\Delta U = U(\text{bulk}) - U(\text{surface})$ between the surface adsorbed configurations and the desorbed bulk configurations (see Figure 7A for an illustration of the two different states). Figure 7B displays the energy differences from the individual interactions of peptide (P), water (W), and surface (S) and their dependence on the side-chain hydrophobicity. The peptides are ordered from left to right according to an increasing side-chain hydrophobicity scale h_S, with shades of blue indicating polar and charged residues and shades of red indicating hydrophobic residues. In agreement with previous results,[16,22] the water−water and peptide−surface interactions are positive (i.e., push the peptide onto the surface) and larger in magnitude than the resulting total energy. Therefore, direct van der Waals interactions, encountered in the peptide−surface contribution, and solvation effects, included via the water−water contribution, are equally important. These positive contributions are canceled by negative contributions of surface−water and peptide−water interactions, which energetically favor the bulk state. The calculated contributions increase with increasing side-chain hydrophobicity for the hydrophobic residues. This increase is directly related to the increasing size of the side chains since a larger side chain enables stronger interaction with surface sites and results in a larger perturbation of the hydrogen bonding network of water. When comparing hydrophobic and charged/polar residues, we find that the single contributions of the polar peptides are larger in magnitude and the resulting total energy is negative. For polar residues the bulk state is thus energetically favored ($U < 0$). The reason for this trend is that polar and charged peptides can interact with water and alter the water structure more efficiently, leading to a maximum total number of hydrogen bonds in the bulk state (see Figure 7D).

Figure 7C displays the total energy U, the free energy A, and the entropic contribution $-TS$ to the adsorption per monomer. Figure 7D shows the difference in the number of hydrogen bonds $\Delta n_{hb} = n_{hb}^{ads} - n_{hb}^{des}$ per monomer in the surface adsorbed n_{hb}^{ads} and the desorbed bulk configuration n_{hb}^{des}. The free energy is positive for all peptides, meaning that the surface adsorbed configuration is favored. The adsorption free energy increases linearly with increasing hydrophobicity as expected from the desorption forces. However, no clear trend is found for the resulting total energy. The combination of the individual contributions into solvent mediated interactions, peptide related contributions, and contribution due to surface solvation are discussed further in the Supporting Information. We can conclude that the adsorption is favored for all peptides considered albeit only very modestly for polar and charge peptides. For hydrophobic peptides, adsorption is favored by the total energy ($U > 0$), and by changes in entropy ($-TS > 0$) upon adsorption. Moreover, the average number of hydrogen bonds is larger in the adsorbed compared to the unbound state in the bulk solvent ($\Delta n_{hb} > 0$). For polar and charged peptides, adsorption is only driven by entropy ($-TS > 0$) and thus is much weaker. Here, the bulk state is energetically favored ($U < 0$) and allows a maximal number of hydrogen bonds ($\Delta n_{hb} < 0$).

Additivity of Adsorption Contributions. Assuming that the contributions to the binding free energy of individual amino acids in a peptide are additive would allow rapid estimation of the total binding free energy of different peptide or protein sequences. For unstructured oligopeptides flatly absorbing to solid surfaces, it has been shown that the binding free energies of amino acid side chains are largely additive.[16,17] In order to test if the additivity assumption is valid for the absorption of peptides at a lipid bilayer, we predict experimental free energy contributions of individual monomers for transfer of a host−guest peptide (AcWL-X-LL) from water to the POPC interface[28] based on our simulation results (Figure 8). In the experiments, the free energy difference for replacing one amino acid by alanine is determined. We predict this value by using our simulation results for homopolypeptides (11−12 residues) and estimate the contribution of each amino acid based on the additivity assumption. Figure 8 shows a comparison of the adsorption free energy per monomer obtained by experiments

DOI: 10.1021/acs.langmuir.5b03435
Langmuir 2016, 32, 810−821

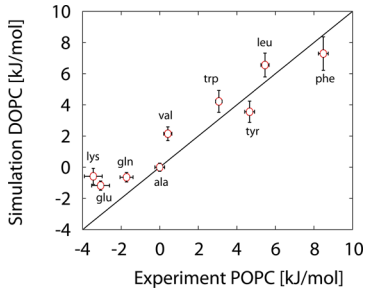

Figure 8. Comparison of simulation results for DOPC (vertical axis) to experimental results for POPC (horizontal axis) for the adsorption free energy normalized to the value of alanine. The experimental free energy difference is determined for replacing a single amino acid in a host–guest peptide by alanine. The experimental values for the contribution of individual amino acids to the binding free energy are compared to our predictions based on the simulation of homopolypeptides and the additivity assumption. The solid line indicates perfect agreement between experiments and simulations. The experimental values are taken from Wimley et al.[28]

and our predictions based on the additivity assumption. The solid line indicates perfect agreement. Although slight deviations are encountered for the charged peptides glutamic acid and lysine, the results of experiments and simulations are overall in excellent agreement. This demonstrates that the contributions of adsorption of individual residues to the total binding free energy are largely additive and that the results from homopolypeptides can be used to estimate the adsorption free energy of unstructured oligopeptides. Moreover, the chemically different structures of DOPC and POPC bilayers do not affect the adsorption at the membrane surface, most likely since the headgroups of the two types of bilayers are identical.

Whether or not peptide attachment to zwitterionic lipid bilayers is driven by a universal mechanism, namely entropy and the maximization of hydrogen bonds, and therefore independent of the chemical structures of the lipid headgroups, needs to be further investigated in the future.

CONCLUSION

We have investigated force-induced desorption of different homopolypeptides chains from phospholipid bilayers with DOPC headgroups by closely matched MD simulations and by AFM experiments. The excellent agreement between the desorption forces found in the experiments and simulations shows that classical simulations with explicit water capture the mechanism underlying reversible attachment of peptides to lipid bilayers. Experimentally, only the sum of the various contributions to the desorption forces can be measured. On the other hand, the simulations allow us to disentangle the various interactions from peptide, surface, and water. Therewith, our combined approach aims at gaining microscopic understanding of the mechanism of reversible peptide attachment to lipid bilayers which is fundamental to the function of peripheral membrane proteins.

Both in simulations and in experiments, hydrophobic peptides preferentially adsorb at the lipid/water interface and the desorption forces increase with increasing side-chain hydrophobicity. When comparing the adsorption of homopeptides with nonpolar side chains, our simulations show that these peptides are driven entropically and energetically to the surface. In addition, the surface adsorbed configuration allows a maximal number of total hydrogen bonds. By contrast, adsorption of charged and polar peptides is energetically disfavored with a net loss of hydrogen bonds. The adsorption of charged/polar peptides to the membrane surface is thus weaker. The key discriminators between weakly adsorbing polar/charged and strongly adsorbing hydrophobic peptides are energetic components due to both solvation effects and direct peptide–surface interactions.

This result is not necessarily expected for the interaction of peptides with a membrane surface since in contrast to a hydrophobic surface it contains a mixture of polar and nonpolar chemical groups. Understanding the adsorption of peptides should be seen as a first step toward the ambitious goal of understanding peripheral membrane protein adsorption to membrane surfaces.

Interestingly, the adsorption free energy per residue obtained from the present simulations on homopeptides shows good agreement with experimental results for single residues in the context of a short pentameric model peptide. It indicates that the free energy contributions of individual residues for peptide binding at membrane surfaces are largely additive. This, however, needs to be tested in future experimental and simulation studies on other peptides and proteins that interact with lipid membrane surfaces. Nevertheless, the present results suggest that detailed studies on model peptides are valuable to derive parameters for predicting the tendency of a protein surface region to potentially interact with a membrane surface and to estimate the associated adsorption or binding free energy. Our study suggests also that one strategy to enhance the adsorption of peripheral membrane proteins is to use patches of hydrophobic residues in the interfacial region.

ASSOCIATED CONTENT

Supporting Information

The Supporting Information is available free of charge on the ACS Publications website at DOI: 10.1021/acs.langmuir.5b03435.

Further discussions of simulated and experimental force–extension curves (PDF)

AUTHOR INFORMATION

Corresponding Author

*E-mail: nschwierz@berkeley.edu.

Notes

The authors declare no competing financial interest.

ACKNOWLEDGMENTS

This work was supported by the Sonderforschungsbereich 863 of Deutsche Forschungsgemeinschaft and performed using supercomputer resources at the Leibniz Center provided by a grant to PRACE Project pr86ri. N.S. thanks the Alexander von Humboldt Foundation for financial support. S.K. and T.H. thank the Elitenetzwerk Bayern in the framework of the doctorate program Material Science of Complex Interfaces and the Nanosystems Initiative Munich (NIM) for financial support.

REFERENCES

(1) Hinderliter, A.; Almeida, P. F. F.; Creutz, C. E.; Biltonen, R. L. Domain Formation in a Fluid Mixed Lipid Bilayer Modulated through Binding of the C2 Protein Motif. *Biochemistry* **2001**, *40*, 4181–4191.

DOI: 10.1021/acs.langmuir.5b03435
Langmuir 2016, 32, 810–821

(2) Cho, W.; Stahelin, R. Membrane-protein interactions in cell signaling and membrane trafficking. *Annu. Rev. Biophys. Biomol. Struct.* **2005**, *34*, 119−151.
(3) Schneider, S. W.; Nuschele, S.; Wixforth, A.; Gorzelanny, C.; Alexander-Katz, A.; Netz, R. R.; Schneider, M. F. Shear-induced unfolding triggers adhesion of von Willebrand factor fibers. *Proc. Natl. Acad. Sci. U. S. A.* **2007**, *104*, 7899−7903.
(4) Ford, M.; Mills, I.; Peter, B.; Vallis, Y.; Praefcke, G.; Evans, P.; McMahon, H. Curvature of clathrin-coated pits driven by epsin. *Nature* **2002**, *419*, 361−366.
(5) Shai, Y. Mechanism of the binding, insertion and destabilization of phospholipid bilayer membranes by alpha-helical antimicrobial and cell non-selective membrane-lytic peptides. *Biochim. Biophys. Acta, Biomembr.* **1999**, *1462*, 55−70.
(6) Butterfield, S. M.; Lashuel, H. A. Amyloidogenic Protein-Membrane Interactions: Mechanistic Insight from Model Systems. *Angew. Chem., Int. Ed.* **2010**, *49*, 5628−5654.
(7) Epand, R.; Vogel, H. Diversity of antimicrobial peptides and their mechanisms of action. *Biochim. Biophys. Acta, Biomembr.* **1999**, *1462*, 11−28.
(8) Conibear, A. C.; Craik, D. J. The Chemistry and Biology of Theta Defensins. *Angew. Chem., Int. Ed.* **2014**, *53*, 10612−10623.
(9) Damodaran, K. V.; Merz, K. M. Interaction of the Fusion Inhibiting Peptide Carbobenzoxy-D-Phe-L-Phe-Gly with N-Methyldioleoylphosphatidylethanolamine Lipid Bilayers. *J. Am. Chem. Soc.* **1995**, *117*, 6561−6571.
(10) Colotto, A.; Martin, I.; Ruysschaert, J.-M.; Sen, A.; Hui, S. W.; Epand, R. M. Structural Study of the Interaction between the SIV Fusion Peptide and Model Membranes? *Biochemistry* **1996**, *35*, 980−989.
(11) Balsinde, J.; Balboa, M.; Insel, P.; Dennis, E. Regulation and inhibition of phospholipase A(2). *Annu. Rev. Pharmacol. Toxicol.* **1999**, *39*, 175−189.
(12) Zhang, S. Fabrication of novel biomaterials through molecular self-assembly. *Nat. Biotechnol.* **2003**, *21*, 1171−1178.
(13) Roach, P.; Farrar, D.; Perry, C. C. Interpretation of Protein Adsorption: Surface-Induced Conformational Changes. *J. Am. Chem. Soc.* **2005**, *127*, 8168−8173.
(14) Rabe, M.; Verdes, D.; Seeger, S. Understanding protein adsorption phenomena at solid surfaces. *Adv. Colloid Interface Sci.* **2011**, *162*, 87−106.
(15) Thyparambil, A. A.; Wei, Y.; Latour, R. A. Determination of PeptideSurface Adsorption Free Energy for Material Surfaces Not Conducive to SPR or QCM using AFM. *Langmuir* **2012**, *28*, 5687−5694.
(16) Schwierz, N.; Horinek, D.; Liese, S.; Pirzer, T.; Balzer, B. N.; Hugel, T.; Netz, R. R. On the Relationship between Peptide Adsorption Resistance and Surface Contact Angle: A Combined Experimental and Simulation Single-Molecule Study. *J. Am. Chem. Soc.* **2012**, *134*, 19628−19638.
(17) Sigal, G. B.; Mrksich, M.; Whitesides, G. M. Effect of Surface Wettability on the Adsorption of Proteins and Detergents. *J. Am. Chem. Soc.* **1998**, *120*, 3464−3473.
(18) Lu, J.; Perumal, S.; Hopkinson, I.; Webster, J.; Penfold, J.; Hwang, W.; Zhang, S. Interfacial nano-structuring of designed peptides regulated by solution pH. *J. Am. Chem. Soc.* **2004**, *126*, 8940−8947.
(19) Pirzer, T.; Geisler, M.; Scheibel, T.; Hugel, T. Single molecule force measurements delineate salt, pH and surface effects on biopolymer adhesion. *Phys. Biol.* **2009**, *6*, 025004.
(20) Kienle, S.; Liese, S.; Schwierz, N.; Netz, R. R.; Hugel, T. The Effect of Temperature on Single-Polypeptide Adsorption. *ChemPhysChem* **2012**, *13*, 982−989.
(21) Chandler, D. Interfaces and the driving force of hydrophobic assembly. *Nature* **2005**, *437*, 640−647.
(22) Horinek, D.; Serr, A.; Geisler, M.; Pirzer, T.; Slotta, U.; Lud, S. Q.; Garrido, J. A.; Scheibel, T.; Hugel, T.; Netz, R. R. Peptide adsorption on a hydrophobic surface results from an interplay of solvation, surface, and intrapeptide forces. *Proc. Natl. Acad. Sci. U. S. A.* **2008**, *105*, 2842−2847.
(23) Sarikaya, M.; Tamerler, C.; Jen, A.; Schulten, K.; Baneyx, F. Molecular biomimetics: nanotechnology through biology. *Nat. Mater.* **2003**, *2*, 577−585.
(24) Absolom, D. R.; Zingg, W.; Neumann, A. W. Protein adsorption to polymer particles: Role of surface properties. *J. Biomed. Mater. Res.* **1987**, *21*, 161−171.
(25) Singh, N.; Husson, S. M. Adsorption thermodynamics of short-chain peptides on charged and uncharged nanothin polymer films. *Langmuir* **2006**, *22*, 8443−8451.
(26) Black, S.; Mould, D. Development of hydrophobicity parameters to analyze proteins which bear posttranslational or cotranslational modifications. *Anal. Biochem.* **1991**, *193*, 72−82.
(27) Wimley, W.; Creamer, T.; White, S. Solvation energies of amino acid side chains and backbone in a family of host-guest pentapeptides. *Biochemistry* **1996**, *35*, 5109−5124.
(28) Wimley, W.; White, S. Experimentally determined hydrophobicity scale for proteins at membrane interfaces. *Nat. Struct. Biol.* **1996**, *3*, 842−848.
(29) White, S.; Wimley, W. Hydrophobic interactions of peptides with membrane interfaces. *Biochim. Biophys. Acta, Rev. Biomembr.* **1998**, *1376*, 339−352.
(30) Hessa, T.; Kim, H.; Bihlmaier, K.; Lundin, C.; Boekel, J.; Andersson, H.; Nilsson, I.; White, S.; von Heijne, G. Recognition of transmembrane helices by the endoplasmic reticulum translocon. *Nature* **2005**, *433*, 377−381.
(31) White, S.; Wimley, W. Membrane protein folding and stability: Physical principles. *Annu. Rev. Biophys. Biomol. Struct.* **1999**, *28*, 319−365.
(32) Aliste, M. P.; MacCallum, J. L.; Tieleman, D. P. Molecular Dynamics Simulations of Pentapeptides at Interfaces: Salt Bridge and Cation Interactions. *Biochemistry* **2003**, *42*, 8976−8987.
(33) MacCallum, J. L.; Bennett, W. F. D.; Tieleman, D. P. Distribution of amino acids in a lipid bilayer from computer simulations. *Biophys. J.* **2008**, *94*, 3393−3404.
(34) Huster, D. Solid-state NMR spectroscopy to study proteinlipid interactions. *Biochim. Biophys. Acta, Mol. Cell Biol. Lipids* **2014**, *1841*, 1146−1160.
(35) Galdiero, S.; Falanga, A.; Cantisani, M.; Vitiello, M.; Morelli, G.; Galdiero, M. Peptide-Lipid Interactions: Experiments and Applications. *Int. J. Mol. Sci.* **2013**, *14*, 18758−18789.
(36) Oliveira, M. D. L.; Franco, O. L.; Nascimento, J. M.; de Melo, C. P.; Andrade, C. A. S. Mechanistic Aspects of Peptide-Membrane Interactions Determined by Optical, Dielectric and Piezoelectric Techniques: An Overview. *Curr. Protein Pept. Sci.* **2013**, *14*, 543−555.
(37) Blume, A.; Kerth, A. Peptide and protein binding to lipid monolayers studied by FT-IRRA spectroscopy. *Biochim. Biophys. Acta, Biomembr.* **2013**, *1828*, 2294−2305.
(38) Naito, A.; Kawamura, I. Solid-state NMR as a method to reveal structure and membrane-interaction of amyloidogenic proteins and peptides. *Biochim. Biophys. Acta, Biomembr.* **2007**, *1768*, 1900−1912.
(39) Marsh, D. Electron spin resonance in membrane research: proteinlipid interactions from challenging beginnings to state of the art. *Eur. Biophys. J.* **2010**, *39*, 513−525.
(40) Meissner, R. H.; Wei, G.; Ciacchi, L. C. Estimation of the free energy of adsorption of a polypeptide on amorphous SiO2 from molecular dynamics simulations and force spectroscopy experiments. *Soft Matter* **2015**, *11*, 6254−6265.
(41) Van Der Spoel, D.; Lindahl, E.; Hess, B.; Groenhof, G.; Mark, A. E.; Berendsen, H. J. C. GROMACS: Fast, flexible, and free. *J. Comput. Chem.* **2005**, *26*, 1701−1718.
(42) Darden, T.; York, D.; Pedersen, L. Particle Mesh Ewald - an N.log(N) method for Ewals sums in large systems. *J. Chem. Phys.* **1993**, *98*, 10089−10092.
(43) Klauda, J. B.; Venable, R. M.; Freites, J. A.; O'Connor, J. W.; Tobias, D. J.; Mondragon-Ramirez, C.; Vorobyov, I.; MacKerell, A. D., Jr.; Pastor, R. W. Update of the CHARMM All-Atom Additive Force Field for Lipids: Validation on Six Lipid Types. *J. Phys. Chem. B* **2010**, *114*, 7830−7843.

DOI: 10.1021/acs.langmuir.5b03435
Langmuir 2016, 32, 810−821

(44) Pastor, R. W.; MacKerell, A. D., Jr. Development of the CHARMM Force Field for Lipids. *J. Phys. Chem. Lett.* **2011**, *2*, 1526−1532.
(45) Vanommeslaeghe, K.; MacKerell, A. D., Jr. CHARMM additive and polarizable force fields for biophysics and computer-aided drug design. *Biochim. Biophys. Acta, Gen. Subj.* **2015**, *1850*, 861−871.
(46) Baker, M. K.; Abrams, C. F. Dynamics of Lipids, Cholesterol, and Transmembrane alpha-Helices from Microsecond Molecular Dynamics Simulations. *J. Phys. Chem. B* **2014**, *118*, 13590−13600.
(47) Chen, L. Y. Computing membrane-AQP5-phosphatidylserine binding affinities with hybrid steered molecular dynamics approach. *Mol. Membr. Biol.* **2015**, *8*, 1−7.
(48) Kucerka, N.; Nagle, J. F.; Sachs, J. N.; Feller, S. E.; Pencer, J.; Jackson, A.; Katsaras, J. Lipid Bilayer Structure Determined by the Simultaneous Analysis of Neutron and X-Ray Scattering Data. *Biophys. J.* **2008**, *95*, 2356−2367.
(49) Katchalsky, A.; Shavit, N.; Eisenberg, H. Dissociation of waek polymeric acids and bases. *J. Polym. Sci.* **1954**, *13*, 69−84.
(50) Netz, R. R. Charge regulation of weak polyelectrolytes at low- and high-dielectric-constant substrates. *J. Phys.: Condens. Matter* **2003**, *15*, S239.
(51) Yesylevskyy, S.; Marrink, S.-J.; Mark, A. E. Alternative Mechanisms for the Interaction of the Cell-Penetrating Peptides Penetratin and the TAT Peptide with Lipid Bilayers. *Biophys. J.* **2009**, *97*, 40−49.
(52) Izrailev, S.; Stepaniants, S.; Balsera, M.; Oono, Y.; Schulten, K. Molecular dynamics study of unbinding of the avidin-biotin complex. *Biophys. J.* **1997**, *72*, 1568−1581.
(53) Evans, E.; Ritchie, K. Dynamic strength of molecular adhesion bonds. *Biophys. J.* **1997**, *72*, 1541−1555.
(54) Noy, A.; Friddle, R. W. Practical single molecule force spectroscopy: How to determine fundamental thermodynamic parameters of intermolecular bonds with an atomic force microscope. *Methods* **2013**, *60*, 142−150.
(55) Hummer, G.; Szabo, A. Kinetics from nonequilibrium single-molecule pulling experiments. *Biophys. J.* **2003**, *85*, 5−15.
(56) Bell, G. Models for the specific adhesion of cells to cells. *Science* **1978**, *200*, 618−627.
(57) Pan, J.; Tristram-Nagle, S.; Kucerka, N.; Nagle, J. F. Temperature Dependence of Structure, Bending Rigidity, and Bilayer Interactions of Dioleoylphosphatidylcholine Bilayers. *Biophys. J.* **2008**, *94*, 117−124.
(58) Krysiak, S.; Liese, S.; Netz, R. R.; Hugel, T. Peptide Desorption Kinetics from Single Molecule Force Spectroscopy Studies. *J. Am. Chem. Soc.* **2014**, *136*, 688−697.
(59) Rubinstein, M.; Colby, R. *Polymer Physics*; Oxford University Press: 2003.
(60) Marko, J. F.; Siggia, E. D. Stretching DNA. *Macromolecules* **1995**, *28*, 8759−8770.
(61) Rief, M.; Oesterhelt, F.; Heymann, B.; Gaub, H. E. Single Molecule Force Spectroscopy on Polysaccharides by Atomic Force Microscopy. *Science* **1997**, *275*, 1295−1297.
(62) Rief, M.; Clausen-Schaumann, H.; Gaub, H. E. Sequence-dependent mechanics of single DNA molecules. *Nat. Struct. Biol.* **1999**, *6*, 346−349.
(63) Oesterhelt, F.; Rief, M.; Gaub, H. E. Single molecule force spectroscopy by AFM indicates helical structure of poly(ethylene-glycol) in water. *New J. Phys.* **1999**, *1*, 6.
(64) Balzer, B. N.; Gallei, M.; Hauf, M. V.; Stallhofer, M.; Wiegleb, L.; Holleitner, A.; Rehahn, M.; Hugel, T. Nanoscale Friction Mechanisms at Solid-Liquid Interfaces. *Angew. Chem., Int. Ed.* **2013**, *52*, 6541−6544.
(65) Yau, W.-M.; Wimley, W. C.; Gawrisch, K.; White, S. H. The Preference of Tryptophan for Membrane Interfaces. *Biochemistry* **1998**, *37*, 14713−14718.
(66) Han, S.; Kim, K.; Koduri, R.; Bittova, L.; Munoz, N.; Leff, A.; Wilton, D.; Gelb, M.; Cho, W. Roles of Trp(31) in high membrane binding and proinflammatory activity of human group V phospholipase A(2). *J. Biol. Chem.* **1999**, *274*, 11881−11888.

DOI: 10.1021/acs.langmuir.5b03435
Langmuir 2016, 32, 810−821